Bulletin of Multi-scale Estimation of Greenhouse Gas Budgets 2023

National Institute for Environmental Studies, Japan
Japan Agency for Marine-Earth Science and Technology, Japan
Meteorological Research Institute, Japan
Chiba University, Japan

National Institute for Environmental Studies
http://www.nies.go.jp

National Institute for Environmental Studies
16-2 Onogawa, Tsukuba, Ibaraki, 305-8506, Japan
Phone: +81-(0)29-850-2827 Facsimile: +81-(0)29-851-2854
E-mail: www@nies.go.jp http://www.nies.go.jp/

March, 2023

Secretariat of Information Collection and Preparation,
United Nations Framework Convention on Climate Change

Dear Sir / Madame,

As an observer institution of the UNFCCC, we would like to submit a short report of national-, regional-, and global-scale greenhouse gas budgets for the purpose of supporting the first Global Stocktake.

Sincerely,

Nobuko SAIGUSA, Ph.D.
Director of Earth System Division,
National Institute for Environmental Studies
E-mail: n.saigusa@nies.go.jp

Synopsis
This bulletin, updated from that submitted last year, provides an overview of the greenhouse gas budgets estimated by the SII-8 project with the aim of contributing to the first Global Stocktake of the Paris Agreement.

1. Introduction

Evaluation of global, regional, national, and local greenhouse gas (GHG) budgets is essential to achieve the climate goal of the Paris Agreement. Unlike the Kyoto Protocol (1997), all parties to the Paris Agreement (2015) are obliged to provide national inventories of anthropogenic GHG emissions and their nationally determined contributions. To ensure transparency, the Paris Agreement authorized the Global Stocktake (GST), which is a process for taking stock of implementations to assess every five years the world's collective progress toward achieving the purpose of the agreement and its long-term goals. The first GST, expected to take place in November 2023, has three components: 1) Information Collection and Preparation, 2) Technical Assessment, and 3) Consideration of Outputs.

This summary report aims to demonstrate the outcomes of research activities in Japan concerning information contributions to the first GST. Funded by the Ministry of the Environment of Japan, the SII-8 strategic research project (Comprehensive Study on Multi-scale Monitoring and Modeling of Greenhouse Gas Budgets) was launched in April 2021. The participating research groups evaluated GHG budgets at multiple scales by using resources such as observational platforms, advanced models, and inventories (Fig. 1). Such efforts are undoubtedly required because the GST should make use of the best available science while taking into consideration equity inputs in a cross-cutting manner. This report presents a brief overview of the methodology adopted in this project and shows the key results that are expected to support the first GST as well as subsequent GSTs. The advantages of the present study come from 1) the integrated deployment of multiple (bottom-up and top-down) approaches, 2) the wide range of spatial scales used, and 3) quick reporting to support decision-making. In particular, the present study thoroughly covers Asian and Pacific areas that other regional or global monitoring activities have covered only sparsely.

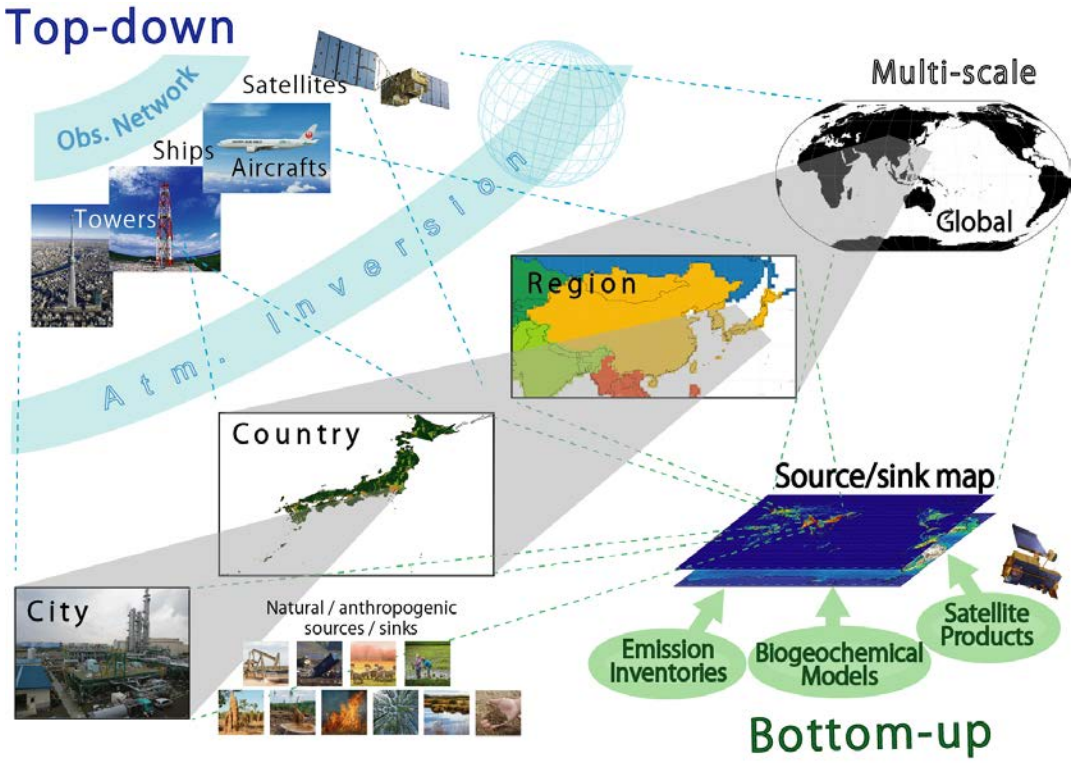

Figure 1. Overview of a multi-scale GHG monitoring system using both top-down and bottom-up approaches.

2. Methodology

2.1. Top-down approach

a) Atmospheric observations

Ground observatories, ships, CONTRAIL (aircraft), GOSAT series (satellites), etc.

The Japan Meteorological Agency (JMA), the Meteorological Research Institute, and the National Institute for Environmental Studies (NIES) monitor atmospheric GHGs from a variety of platforms, including from ground sites (Watanabe *et al*., 2000; Mukai *et al*., 2001; Tohjima *et al*., 2002; Tsutsumi *et al*., 2006), JMA research vessels (Ishii *et al*., 2011; Ono *et al.*, 2019), commercial cargo ships (Terao *et al*., 2011; Tohjima *et al*., 2012), aircraft (Machida *et al*., 2008; Matsueda *et al*., 2008; Tsuboi *et al*., 2013; Umezawa *et al*., 2020), and satellites (Yokota *et al*., 2009; Yoshida *et al*., 2013) (Fig. 2). Measurements of GHGs are made on site or in air samples that are collected in canisters and sent back to individual laboratories. Laboratory analyses determine the mole fractions of the GHGs and their isotopic composition. The mole fractions of the GHGs, including CO_2, CH_4, and N_2O, are precisely determined based on highly compatible standard scales (Tsuboi *et al*., 2017). Time series of CO_2 and CH_4 concentrations over the Asia-Pacific region from 2010 through 2022 (Fig. 3) show spatiotemporal variability at background (e.g., MNM), continental (e.g., NTL), and urban (e.g., YYG) sites. After strict quality assurance and quality control procedures, these observation data are provided directly to atmospheric inversion systems.

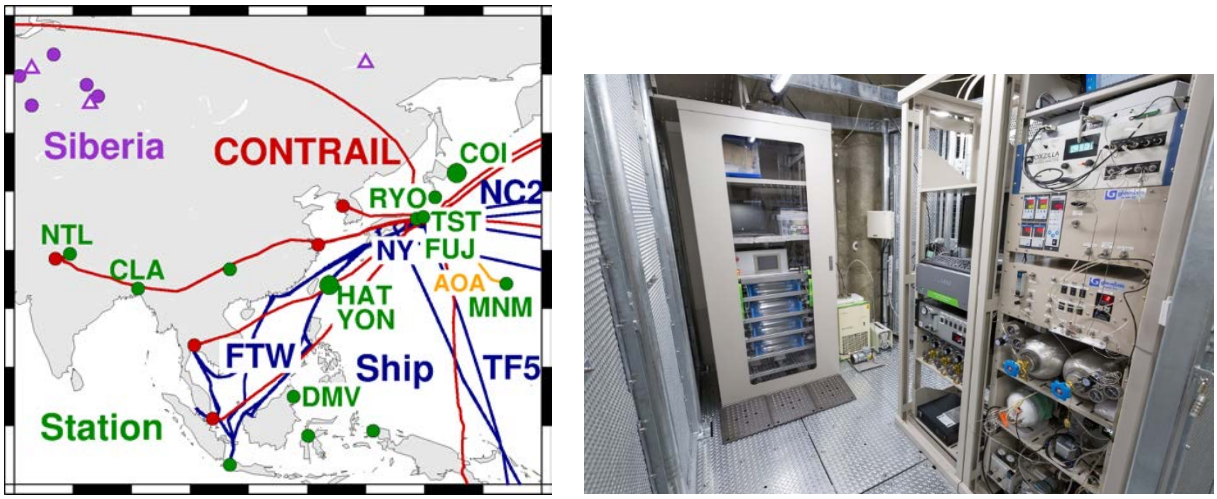

Figure 2. (left) Map showing the locations of atmospheric GHG observations in the Asia-Pacific region. Green circles represent ground site locations, blue lines indicate ship routes, and red lines indicate aircraft flight routes. (right) Photograph showing atmospheric observation systems at a broadcasting tower (Tokyo Skytree) in the Tokyo megacity.

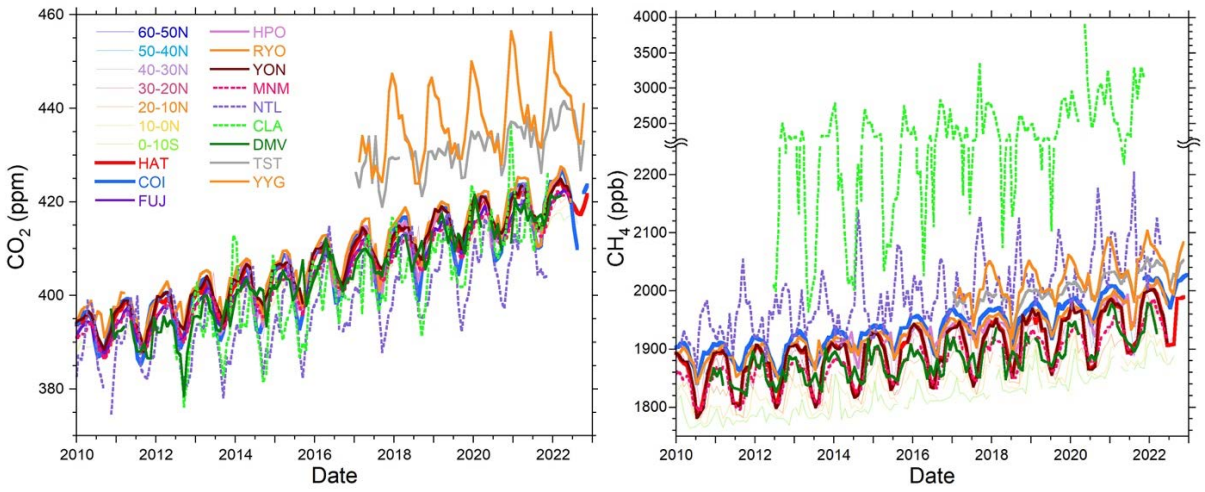

Figure 3. Monthly time series of atmospheric CO_2 (left) and CH_4 (right) concentrations observed over the Asia-Pacific region from 2010 through 2022.

NIES has been conducting atmospheric GHG observations from a cargo ship named *Nichiyu Maru* belonging to Kagoshima Senpaku Co. (Fig. 4(a)) since 2022. The ship makes a round trip between Kawasaki (Kanagawa Pref.) on the main island of Japan (Honshu) and Karita (Fukuoka Pref.) in the Kyushu region in one week and calls at various ports, including Toyohashi, Nagoya, and Kobe, in between. As an example, the spatial distribution of the atmospheric CO_2 concentration observed from 5 to 12 May 2022 (Fig. 4b) along the ship track shows large variability, ranging from 415 ppm to 500 ppm. In addition, NIES has obtained temporal CO_2 variations, especially in the ports of call, that imply that a relationship exists between the size of the urban area around a port and CO_2 variations. These observed data are useful for validating GHG emissions in cities.

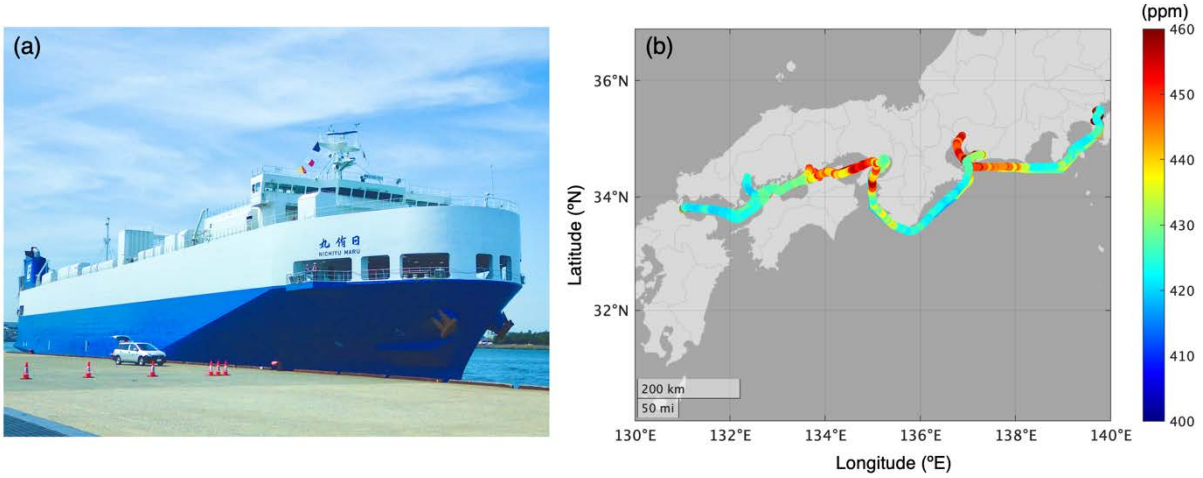

Figure 4. (a) Photograph of *Nichiyu Maru* and (b) the spatial distribution of the atmospheric CO_2 concentration observed from 5 to 12 May 2022 along the ship track.

b) Atmospheric inversion modeling

NICAM-TM and NISMON:

The Nonhydrostatic Icosahedral Atmospheric Model (NICAM) is a numerical simulation model developed for global high-resolution simulations by the University of Tokyo, the Japan Agency for Marine-Earth Science and Technology (JAMSTEC), RIKEN, and other Japanese institutes (Satoh *et al*., 2014). The NICAM-based Transport Model (NICAM-TM) and the NICAM-based Inverse Simulation for Monitoring greenhouse gases (NISMON) are used to simulate concentration variations of CO_2 and CH_4 in the atmosphere and estimate the surface fluxes of these gases (Niwa *et al*., 2017a,b, 2022). NICAM-TM was developed for GHG studies in a study by Niwa *et al*. (2011). In NISMON, the four-dimensional variational method, a state-of-the-art data assimilation/inversion method, is implemented to exploit the large number of observations and estimate high-resolution (model grid point) flux values (i.e., large-dimensional problems) (Niwa *et al*., 2017a,b). Its application to the estimation of CO_2 fluxes (NISMON-CO_2) was demonstrated by Niwa *et al*. (2021). Long-term analyses, which are conducted once a year, with several updates since 2020 (Niwa, 2020), are used in syntheses of the global carbon cycle prepared by the Global Carbon Project (GCP; Friedlingstein *et al*., 2022). The prior fluxes of NISMON-CO_2 v2021.1 consist of fossil fuel emissions from the Gridded fossil CO_2 emission database GCP-GridFED (Jones *et al*., 2021); terrestrial biosphere fluxes from a process-based terrestrial ecosystem model, the Vegetation Integrative SImulator for Trace gases (VISIT; Inatomi *et al*., 2010, Ito and Inatomi, 2012, Ito, 2019); a satellite-based biomass burning emissions product, the Global Fire Emissions Database (GFED) v4.1s (van der Werf *et al*., 2017); and shipboard measurement-based ocean flux data from the JMA (Iida *et al*., 2021).

MIROC4-ACTM:

The Model for Interdisciplinary Research on Climate, version 4 (MIROC4), is an Earth system model (ESM) developed at JAMSTEC, in collaboration with the University of Tokyo and NIES. MIROC4-ACTM is the atmospheric chemistry transport version of MIROC4 (Patra *et al*., 2018). Simulations of long-lived gases in the atmosphere (CO_2, CH_4, N_2O, SF_6) are performed with spectral truncation T42 as the horizontal resolution (~2.8° latitude × ~2.8° longitude grid) with 67 vertical hybrid-pressure layers

between the Earth's surface and 0.0128 hPa (~80 km). The simulated horizontal winds (U, V) and temperature (T) are nudged with JMA's reanalysis data product (JRA-55; Kobayashi *et al*., 2015) over the altitude range of ~980 to 0.018 hPa for better representation of atmospheric transport at synoptic and seasonal timescales. We tested the large-scale interhemispheric transport and Brewer–Dobson circulation in MIROC4-ACTM using SF_6 simulations in the troposphere and the CO_2-derived age of air in the troposphere and stratosphere (Patra *et al*., 2018; Bisht *et al*., 2021; and references therein). The MIROC4-ACTM inversion system optimizes monthly mean fluxes from 84 regions of the globe for CO_2 and N_2O (Saeki and Patra, 2017; Patra *et al*., 2022) and 54 land regions for CH_4 (updated from Chandra *et al*., 2021). This year's MIROC4-ACTM inversions are performed using two sets of prior fluxes for land and ocean, and by varying the prior flux uncertainty (PFU) and measurement data uncertainty (MDU) (similar to Chandra *et al*., 2022, but for a smaller number of PFU and MDU cases). The major difference from last year's report is in the treatment of fossil fuel emissions (which are considered as known by CO_2 inversion systems).

2.2. Bottom-up approach

This approach uses emission inventories, biogeochemical models, and surface remote sensing data to evaluate individual GHG sinks and sources (Fig. 5), and is therefore independent of atmospheric observational data. Compared with the top-down approach, the bottom-up approach has the advantages of greater spatial resolution and sectorial explicitness, but disadvantages due to a reporting time lag and data-specific uncertainties. In general, the bottom-up approach uses multiple data sources to cover a variety of sinks and sources in both natural and anthropogenic sectors. In this project, we mainly use a biogeochemical model to estimate GHG sources and sinks of natural sectors and an emission inventory for anthropogenic emissions. Because the simulation of wildfire is highly uncertain in the biogeochemical model, a satellite-derived product is used for wildfire emissions.

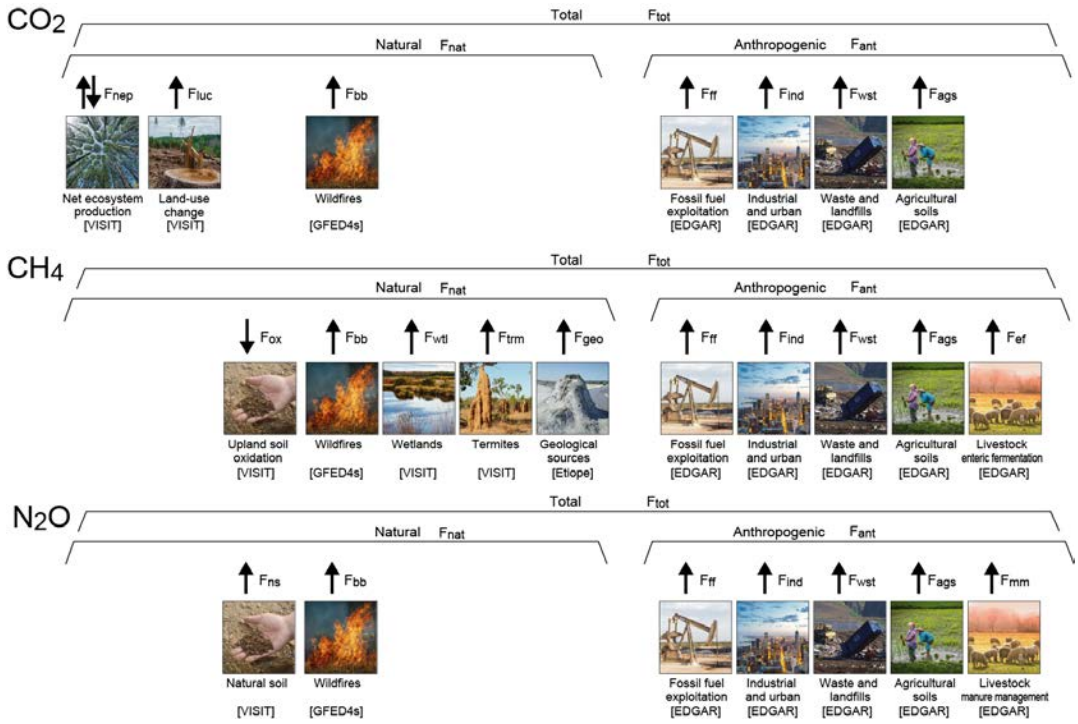

Figure 5. Summary of the bottom-up estimation of GHG budgets: CO_2 (top), CH_4 (middle), and N_2O (bottom). The method and data used to estimate each flow are shown in [brackets].

a) Biogeochemical model

The process-based terrestrial ecosystem model VISIT was used to simulate the GHG exchange of natural and agricultural ecosystems. This model, which consists of biogeophysical (e.g., radiation budget) and biogeochemical schemes and simulates water, carbon, and nitrogen cycles, has been used in regional and global studies of terrestrial GHG budgets and has been validated by using atmospheric and field

measurement data (e.g., Patra *et al*., 2011, 2022; Chandra *et al*., 2021). VISIT returns the total flux at each grid point as area fraction-weighted values. In the cropland fraction, agricultural practices such as planting, harvesting, and fertilizer input are considered in a simplified manner (Ito *et al*., 2018).

b) Emission inventories and satellite products

Anthropogenic emission database

Anthropogenic emission inventories were used for the bottom-up estimation, as well as prior data of atmospheric inversions. Specifically, the Emission Database for Global Atmospheric Research (EDGAR; Crippa *et al*., 2020) version 6.0 was used because this dataset covers all GHGs and has a high spatial resolution (0.1° × 0.1°) and explicit sectorial classification. The emission sectors were aggregated into four to five categories: fossil fuel mining; urban and industry; waste, including landfills; agriculture; and indirect emissions (N_2O from deposition) or livestock (CH_4 only). For comparison, several other emission datasets were referred to: the Open-Data Inventory for Anthropogenic Carbon dioxide (ODIAC), GridFED, FAOSTAT for agricultural emissions, GAINS/IIASA for CH_4 and N_2O, and the Community Emissions Data System (CEDS).

Fire emission database

Biomass burning emissions of CO_2, CH_4, and N_2O were derived from GFED v4s (van der Werf *et al*., 2017), which includes small fires. Emission factors (i.e., emissions per unit weight of biomass burning) were derived from Akagi *et al.* (2011). Because of uncertainties in burnt-area detection algorithms and emission factors, the GFEDv4s-based biomass burning emissions should be evaluated by comparing them with those of similar products such as GFAS (Global Fire Assimilation System) and FINN (Fire Inventory from NCAR).

2.3. Earth System Models

To quantitatively assess the extent to which each country's efforts to reduce GHG emissions will lead to global warming mitigation, we performed climate projections using ESMs with different levels of complexity.

a) MIROC-ES2L

The MIROC-ES2L ESM (Hajima *et al.*, 2020) is used for the climate projections in this study. This model was intensively used for performing the Coupled Model Intercomparison Project Phase 6 (CMIP6) experiments. Because simulated CO_2 concentrations are still biased in the current generation of ESMs and it was necessary to improve their accuracy for near-term climate and carbon cycle simulations, the model was modified to capture the observed global CO_2 concentration by introducing a "nudging" system.

b) FaIR v1.6.4

A simplified climate model was also used to emulate the climate–carbon cycle processes simulated by the full ESM. The FaIR emulator, version 1.6.4 (Millar *et al*., 2017; Smith *et al*., 2018), which was widely used for the last IPCC report, was used here. This model supports the ESM's simulations by extending them to include simulations forced by different emission scenarios. The model parameters for physical climate and carbon cycle processes were automatically determined by a nonlinear least squares method. The treatment of other climate change drivers such as aerosols and air pollutants follows Nicholls *et al*. (2020).

3. Greenhouse gas budgets

3.1. Top-down approach

a) Global, regional, and national budgets

Figure 6 shows trends in CO_2 fluxes in four, semi-hemispheric latitude bands estimated by MIROC4-ACTM inversion systems for the period 2000–2021. In general, when fossil fuel emissions were increasing at the fastest rate during 2002–2010, the inversion-estimated land sink also increased. Saeki and Patra (2017) previously highlighted a similar emission–sink link for the East Asia region by a joint analysis of CO_2 and CH_4 inversion results, but they did not perform a detailed analysis because of a lack of information on the fossil fuel emission uncertainty. Since then, the upper and lower bounds of gridded

fossil fuel emissions have become available in GridFED (Jones *et al*., 2022). In Fig. 6, large and persistent biases in fossil fuel emissions (column a) are seen in the northern extratropical latitudes (north of 30°N; top row) and, thus, in compensating residual land sinks (column b). In the northern tropical latitudes (Equator to 30°N; 2nd row from top), a difference in the rate of increase of fossil fuel emissions is seen and a similarly compensating change in land flux rates. In the southern tropics (3rd row) and southern extratropics (4th row), no significant fossil fuel emission and residual flux estimates are seen.

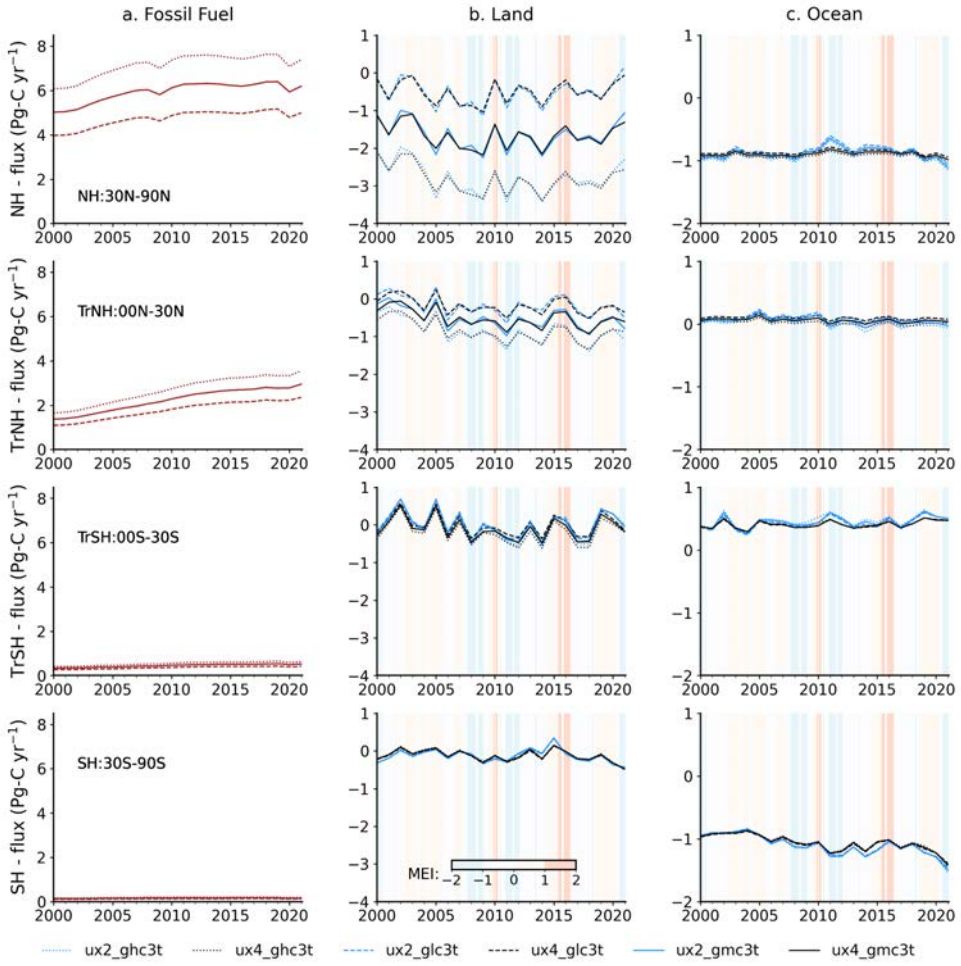

Figure 6. Semi-hemispheric annual CO_2 emissions from fossil fuels (a: dotted line: upper bound; dashed line: lower bound; solid line: mean), and corresponding land (b) and ocean (c) carbon sinks estimated by MIROC4-ACTM inverse modelling. The background shading shows multivariate ENSO index (MEI) values. The blue and black lines are for two different observational data uncertainties in the inversions (ux2 and ux4, see legends) corresponding to upper bound, lower bound and mean fossil fuel emissions (dotted, dashed, and solid curves, respectively).

In Fig. 7, which shows the effects of fossil fuel emissions on sub-continental scale fluxes, it is clear that the land fluxes estimated by MIROC4-ACTM inversions are clearly closely coupled to differences in the assumed fossil fuel emissions. The most significant differences are found in East Asia, which is dominated by the uncertainty in China's fossil fuel emissions. In most other regions, the curves for the estimated land fluxes for the mean and upper and lower fossil fuel emission levels are parallel; thus, the land fluxes estimated by different inversions show similar interannual variabilities and trends. In East Asia, the fossil fuel emission uncertainty was about ±0.3 Pg C yr^{-1} in 2000 and increased to about ±0.7 Pg C yr^{-1} in 2021. Accordingly, the estimated land fluxes exhibit large differences in how the land sink in East Asia changed during 2002–2010. The CO_2 sink increased by as much as 0.5 Pg C yr^{-1} in the short period from 2001 to 2009 when the upper bound of fossil fuel emissions was used (Fig. 7, panel (m)). These results have large implications for the development of ESMs, particularly for the prediction of carbon-climate responses, and for tracking of CO_2 sinks in individual countries.

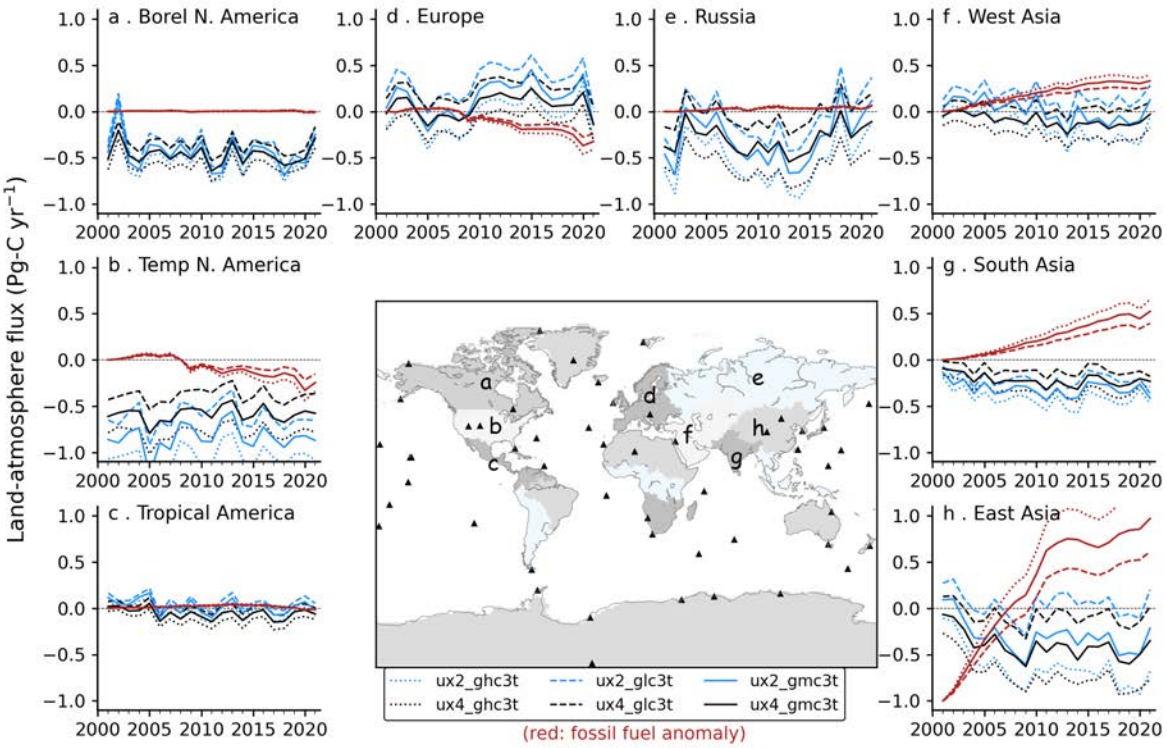

Figure 7. Regional CO_2 fluxes for eight land regions estimated by using different fossil fuel emissions in MIROC4-ACTM inversions. Six inversion runs (see legends) were conducted using 2 different observation data uncertainties (ux2 and ux4 in the legends) for 3 different cases of fossil fuel CO_2 emission anomalies (red lines; showing the mean (solid), lower bound (dashed) and upper bound (dotted)). The fossil fuel emission anomalies for East Asia are offset by –1 Pg C yr^{-1} for fitting in to a common y-axis range (panel h).

Figure 8 shows CH_4 emission anomalies in 15 land regions for the period 2001–2021. We took advantage of a joint analysis of region-specific bottom-up emissions for a few dominant sources and regional total top-down emissions to assess the causes of CH_4 growth rate variabilities during decreasing (1990–1998), quasi-stationary (1999–2005), and regrowth (post-2006) phases. In general, the top-down emission trends agree well with bottom-up emission trends, except for a prominent mismatch in East Asia after 2002; this result suggests that inventory emissions are in overall agreement with the observed CH_4 concentrations for the control case without chemical loss (i.e., no interannual variability in the hydroxyl (OH) concentration). The agreement between bottom-up and top-down estimates seen here should not be interpreted as a drawback of the inversion but rather as an improvement in the a priori emissions, and the bottom-up and top-down emission estimates provide complementary information for better policymaking. To emphasize this point we have run CH_4 inversions using 4 different prior cases, 1) Post_Inv1: same as those provided by the GCP-CH_4 project, 2) Post_Inv7: same as 1) + freshwater emission of 46 Tg-CH_4 yr^{-1}, 3) Post_vCao: same as 1) but the wetland emissions are taken from VISIT Cao scheme, and 4) Post_viWH: same as 1) but the wetland emissions are taken from VISIT Walter-Heimann scheme. All inversions estimated similar CH_4 emission anomalies that are in agreement of the long-term anthropogenic emission trends in GCP-CH_4 a priori (Fig. 8). The long-term mean posteriori emissions (given within each panel) are closer for all 4 inversions compared to the a priori emissions for most regions. One of the highlights of this year's Bulletin is that the MIROC4-ACTM inversions suggest the global total CH_4 emissions exceeded 600 Tg CH_4 yr^{-1} in 2020, from a total of less than 550 Tg CH_4 yr^{-1} in 2005 (Table 1). The MIROC4-ACTM inversion results are significantly lower than the bottom-up estimations (Table 2).

Many of the land regions show large interannual variability and systematic increases in predicted N_2O emissions during 1997–2019 (Fig. 9, colored lines), and for most regions, the systematic increases are in phase with the prior emission scenarios (gray lines). This result suggests that the VISIT model, driven by fertilizer input data from FAOSTAT, simulates well the N_2O emissions from agricultural activities. The

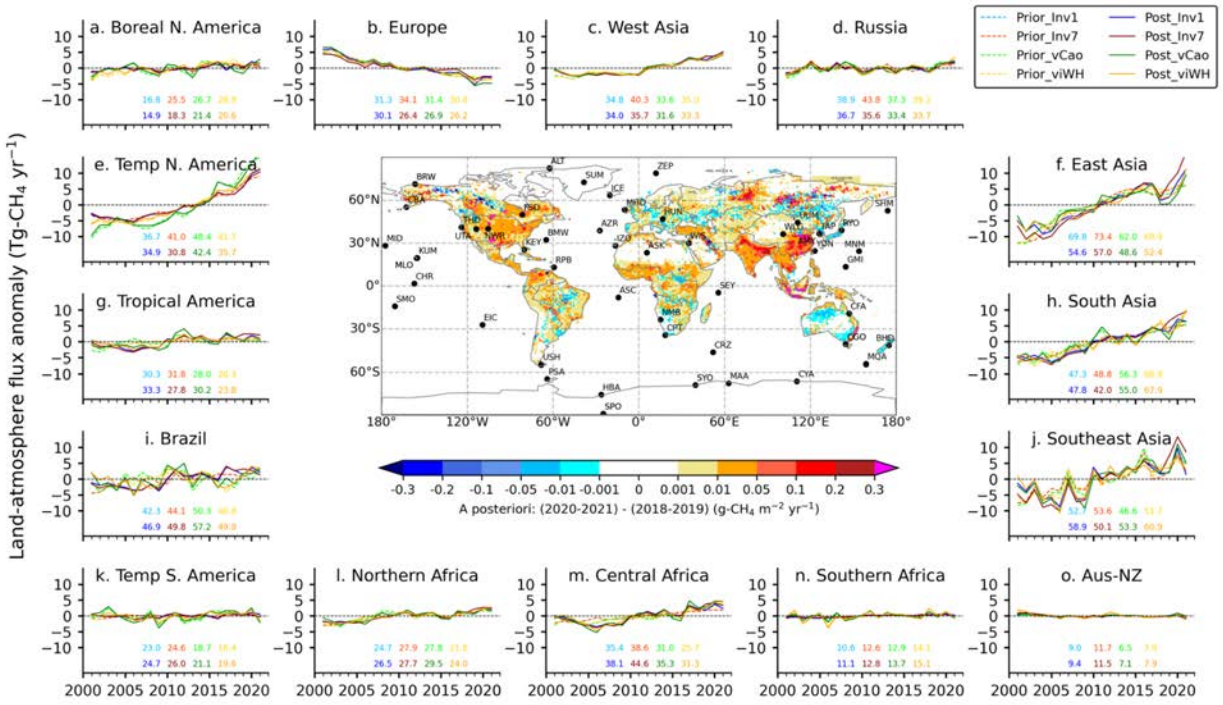

Figure 8. Time series (2003–2021) of regional CH_4 emission anomalies as estimated by two MIROC4-ACTM inversion cases (lines, mean values; shading, the spread of the two cases). The map of emission changes between 2020–2021 and 2018–2019 shows the boundaries between the 15 regions (black lines) and the locations of 60 sites (black circles). The long-term (2003–2021) means of individual inversion cases for each region were subtracted from the global mean to calculate the emission anomalies (long-term mean numbers in each panel, in Tg yr^{-1}). Plot adapted from Chandra *et al.* (2021) and updated by Dmitry Belikov, Chiba University, by extending the period of inversion until 2021.

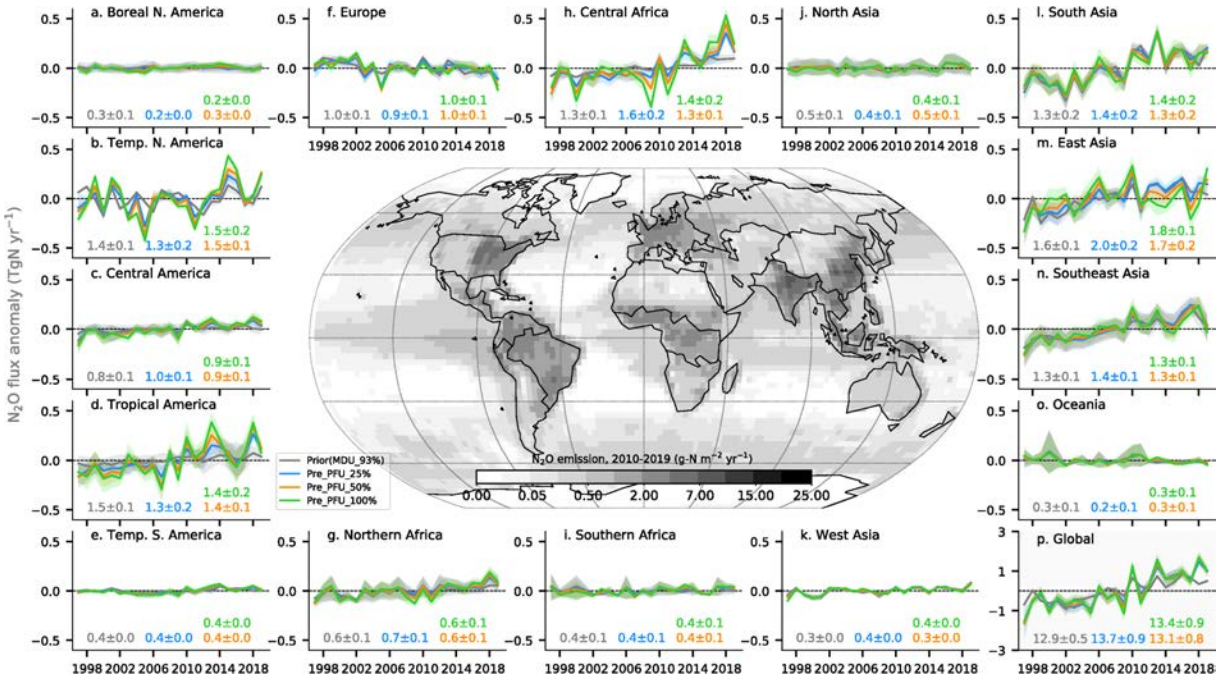

Figure 9. Regional N_2O emissions from the 15 land regions (delineated by black lines on the 2010s mean emission map) for three bottom-up (gray) and three top-down emissions cases in which the prior flux uncertainty was varied (PFU cases: 25%, blue; 50%, orange; and 100%, green). All top-down results correspond to the case of MDU = 93% (details in Patra *et al.*, 2022). The long-term (1997–2019) mean regional emissions (numbers within each panel) were subtracted from the annual mean emission, and the 1-sigma standard deviation (shaded area) was calculated from the different a priori cases. The map in the center shows gridded N_2O emissions. Plot taken from Patra *et al*. (2022).

notable exceptions are the Tropical America and Central Africa regions, where the rates of predicted emission increases are at least twice the prior emission increase rate (Fig. 9d, h). Our results confirm that N_2O emissions from Europe were reduced over the period of this analysis. This emission reduction was due to the adoption of modern technology by the chemical industry, which manufactures nitric acid, mainly for fertilizer production, and adipic acid for nylon production (ref. EDGAR). Similar reductions in N_2O emissions from Japan are also reported in inventory estimates. With this year's update of the bottom-up N_2O emissions a better agreement with top-down estimation is achieved for the East Asia region (Table 2). However, the gap between the global total emissions for the top-down and bottom-up emissions has increased.

b) Near-real-time estimation of fossil fuel-derived CO_2 emissions from China based on atmospheric observations at stations HAT and YON

The atmospheric CO_2 and CH_4 mole fractions observed at Hateruma Island (HAT, 24.06°N, 123.81°E) and Yonaguni Island (YON, 24.47°N, 123.01°E) frequently showed relatively large and correlative synoptic-scale variations from late autumn to early spring because continental air masses with elevated CO_2 and CH_4 concentrations are often transported to these islands during those seasons under the influence of the East Asian monsoon. Previous studies have revealed that the variability ratio of CO_2 and CH_4 ($\Delta CO_2/\Delta CH_4$ ratio) at HAT and YON during the winter period is a good indicator of the change in relative emission strengths in China (Tohjima *et al*., 2014, 2020, 2022). In fact, the monthly average $\Delta CO_2/\Delta CH_4$ ratios during three months (January, February, and March) increased gradually from 2000 to 2010, when Chinese economic activity showed unprecedented growth. In addition, the $\Delta CO_2/\Delta CH_4$ ratio showed an abrupt decrease in February 2020, when a considerable reduction in the fossil fuel-derived CO_2 ($FFCO_2$) emissions caused by the severe nationwide lockdown in China was estimated.

Taking into account the above facts, we have developed a near-real-time estimation method for CO_2 emissions from China that uses the atmospheric $\Delta CO_2/\Delta CH_4$ variability ratio at HAT and YON (Tohjima et al. 2023). We simulated atmospheric CO_2 and CH_4 using an atmospheric transport model (NICAM-TM, Niwa *et al*., 2011) and a full set of surface CO_2 and CH_4 fluxes and found a linear relationship between simulated $\Delta CO_2/\Delta CH_4$ ratios and $FFCO_2/CH_4$ emission ratios in China during January, February, and March. Therefore, we could use this linear relationship to convert the observed $\Delta CO_2/\Delta CH_4$ ratios to $FFCO_2/CH_4$ emission ratios in China. Then, we calculated the change rate of the $FFCO_2/CH_4$ emission ratios compared to the corresponding averages for the preceding 9-year period (2011–2019), during which relatively stable $\Delta CO_2/\Delta CH_4$ ratios were observed. Under the additional assumption that there were no interannual variations in biospheric CO_2 and CH_4 fluxes, we can interpret the rate of change in the

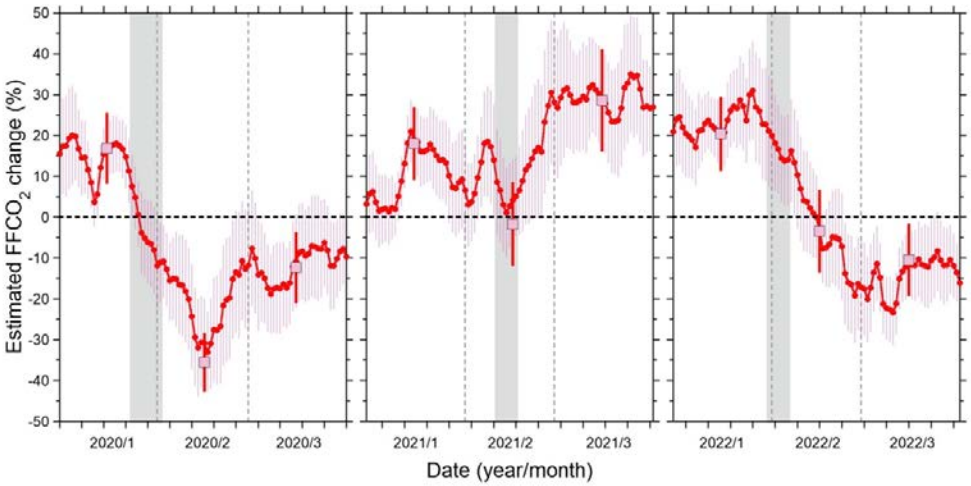

Figure 10. Estimated $FFCO_2$ emission changes in China based on the $\Delta CO_2/\Delta CH_4$ ratios observed at HAT and YON. The estimated results for January, February, and March in 2020, 2021, and 2022 compared to the preceding 9-year average are depicted in the left, middle, and right panels, respectively. The red circles with red lines and pink squares represent estimates based on 30-day moving averages and monthly averages, respectively, of the observed $\Delta CO_2/\Delta CH_4$ ratio. The vertical bars represent uncertainties. The vertical gray-shaded bars correspond to the Chinese New Year holiday.

$FFCO_2/CH_4$ emission ratio as the rate of change in $FFCO_2$ emissions from China. Finally, we computed the weighted averages of the estimated change rates for HAT and YON.

Using the method described above, we estimated the change in $FFCO_2$ emissions from China for 2020, 2021, and 2022 compared to the preceding 9-year average (Fig. 10). The resulting changes in $FFCO_2$ emissions for January, February, and March (JFM) were 17 ± 8%, −36 ± 7%, and −12 ± 8%, respectively, in 2020 (−10 ± 9% for JFM overall), 18 ± 8%, −2 ± 10%, and 29 ± 12%, respectively, in 2021 (15 ± 10% for JFM overall), and 20 ± 9%, −3 ± 10%, and −10 ± 9%, respectively, in 2022 (2 ± 9% for JFM overall). Our estimation results suggest that $FFCO_2$ emissions from China, which decreased considerably during February 2020, rebounded with the recovery of socioeconomic activity in China after the COVID lockdown. However, the slight decrease in our estimated $FFCO_2$ change in March 2022 suggests that the $FFCO_2$ emissions from China were still being affected in 2022 by the COVID-19 infection status in China.

c) Estimation of net CO_2 flux from the Tokyo megacity using NICAM-TM and observations at Tokyo Skytree

Using NICAM-TM with the inversion flux data from NISMON-CO_2 and observations at Tokyo Skytree, we estimated the net CO_2 flux from the Tokyo megacity. Here, the inversion flux data were downscaled from 1° × 1° to the high-resolution NICAM grid (~14 km) to better resolve the Tokyo area in the model. However, there was a significantly large discrepancy between the simulation results and the observations at Tokyo Skytree (Fig. 11, center top panel). This discrepancy can be attributed to the use of incorrect emission data and the still-insufficient representativeness of the model; the contribution of the latter can be eliminated by data selection with meteorological data. Then, the net CO_2 flux from Tokyo can be estimated by comparing simulation results with observations from which simulated background concentrations have been subtracted. The simulated background concentrations, which are derived from areas other than Tokyo, are considered to be nearly true because inversion flux data globally optimized by worldwide observations are used (see the good agreement between the model and observations at Minamitorishima, a background station; Fig. 11, center bottom panel).

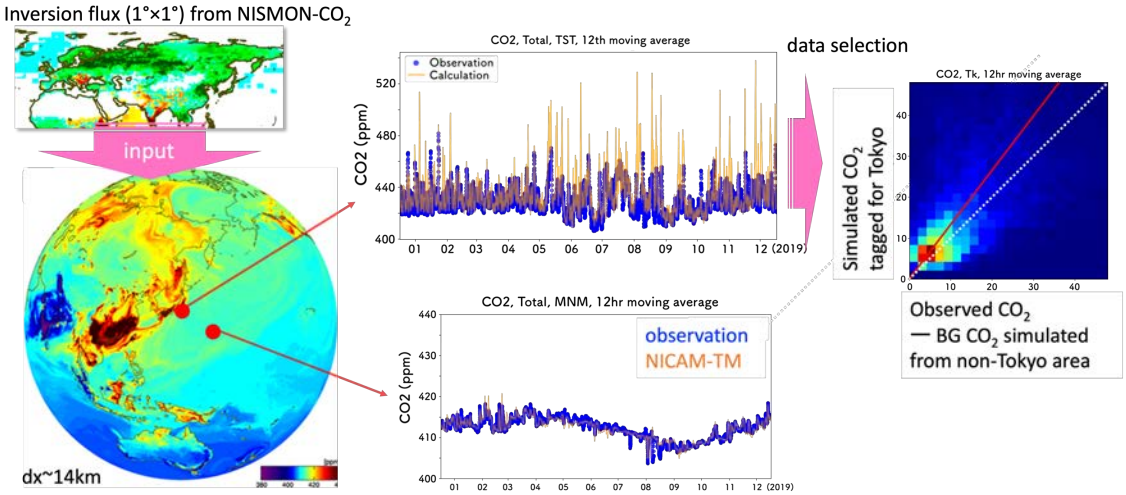

Figure 11. Schematic diagram of CO_2 flux estimation for the Tokyo megacity. The inversion flux from NISMON-CO_2 and the surface CO_2 concentration field simulated by NICAM-TM with a 14-km resolution are shown on the left. In the center, simulation results are compared with observations at Tokyo Skytree (top) and Minamitorishima (MNM; bottom). On the right, Tokyo-originated concentrations are compared between the model and observations. The Tokyo-originated concentrations are derived by subtracting background concentrations simulated in non-Tokyo areas from the observed concentrations.

3.2. Bottom-up approach

The bottom-up approach provides global maps of sources and sinks for each of the GHGs and sectors (Fig. 4). By aggregating the maps, global, regional (e.g., East Asia), and national (e.g., Japan) GHG budgets were obtained. Note that this procedure is applicable to any region and country and allows us to obtain consistent budgets across scales, because the global budget is equal to the sum of the regional and country-based budgets.

a) CO_2 budget (2001–2021)

Global: Anthropogenic emissions were estimated to be 36,488 Tg CO_2 yr^{-1}, of which the industrial and urban sector (F_{ind}) played a dominant role. The natural budget was estimated to be a net sink of –17,730 Tg CO_2 yr^{-1}, mainly due to growth in terrestrial ecosystems (F_{nep}).

Regional (East Asia): Anthropogenic emissions were estimated to be 10,993 Tg CO_2 yr^{-1}, mainly attributable to a rapid increase of industrial and urban emissions in China (9,054 Tg CO_2 yr^{-1}). The natural budget was a net sink of –1961 Tg CO_2 yr^{-1}.

National (Japan): Anthropogenic emissions were estimated to be 962 Tg CO_2 yr^{-1}, and they peaked around 2013. The natural budget was a net sink of 156 Tg CO_2 yr^{-1} because of growing forests (Fig. 12).

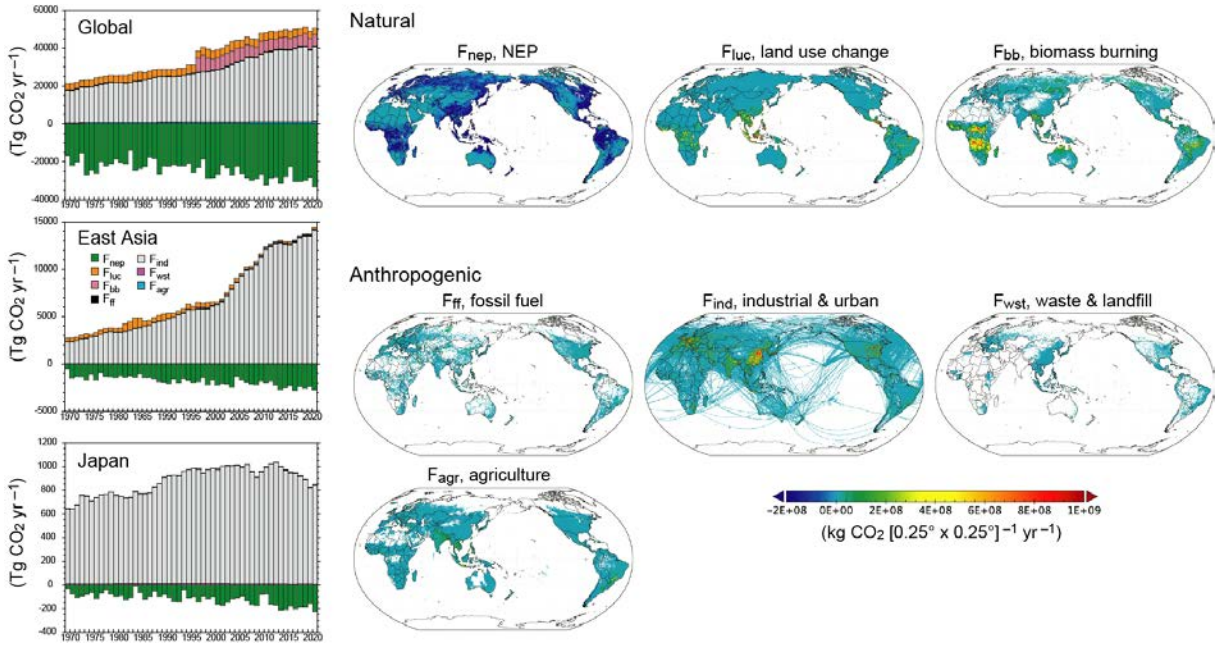

Figure 12. CO_2 budgets estimated by the bottom-up approach. The maps show mean annual budgets during 2001–2021.

b) CH_4 Budget (2001–2021)

Global: Anthropogenic emissions were estimated to be 320.6 Tg CH_4 yr^{-1}, in which the industrial and urban sector (F_{ind}) played a dominant role. The natural budget was estimated to be a net source of 172.0 Tg CH_4 yr^{-1}, mainly due to wetland emissions (F_{wet}).

Regional (East Asia): Anthropogenic emissions were estimated to be 65.1 Tg CH_4 yr^{-1}, reflecting a rapid increase in fossil fuel exploitation (F_{ff}) in China (from 8.8 to 15.9 Tg CH_4 yr^{-1}). The natural budget was a weak net source of 4.4 Tg CH_4 yr^{-1}.

National (Japan): Anthropogenic emissions were estimated to be 1.99 Tg CH_4 yr^{-1} and showed a gradual decrease. The natural budget was a net source of 0.7 Tg CH_4 yr^{-1} from wetlands and geological sources (F_{geo}) (Fig. 13).

c) N_2O budget (2001–2021)

Global: Anthropogenic emissions were estimated to be 8.4 Tg N_2O yr^{-1}, in which the agricultural sector (F_{ags}) played a dominant role. The natural budget was estimated to be a net source of 10.1 Tg N_2O yr^{-1}, due mainly to natural soil emissions (F_{ns}).

Regional (East Asia): Anthropogenic emissions were estimated to be 1.6 Tg N_2O yr^{-1}, reflecting a rapid increase in agricultural fertilizer use from 1970 in China. The natural budget was a moderate net source of 0.7 Tg N_2O yr^{-1}.

National (Japan): Anthropogenic emissions were estimated to be 0.06 Tg N_2O yr^{-1}, and they gradually decreased from 1999. The natural budget was a weak net source of 0.04 Tg N_2O yr^{-1} from natural soils (Fig. 14).

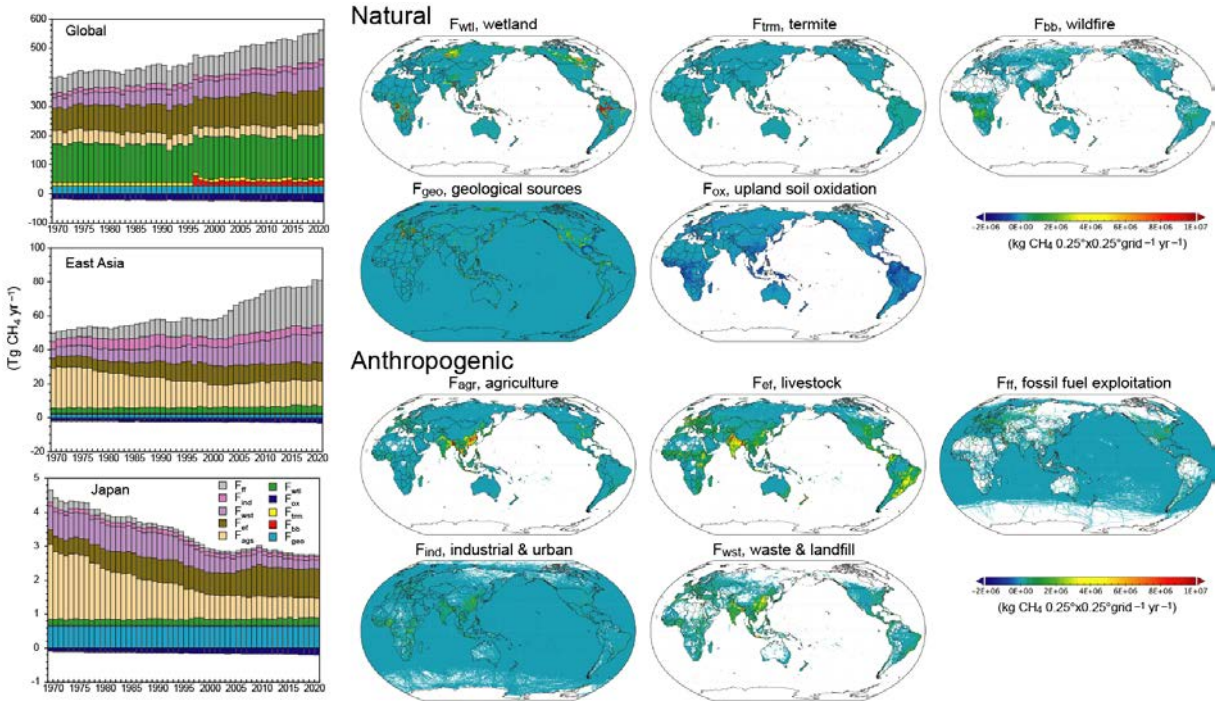

Figure 13. CH_4 budgets estimated by the bottom-up approach. The maps show mean annual budgets during 2001–2021.

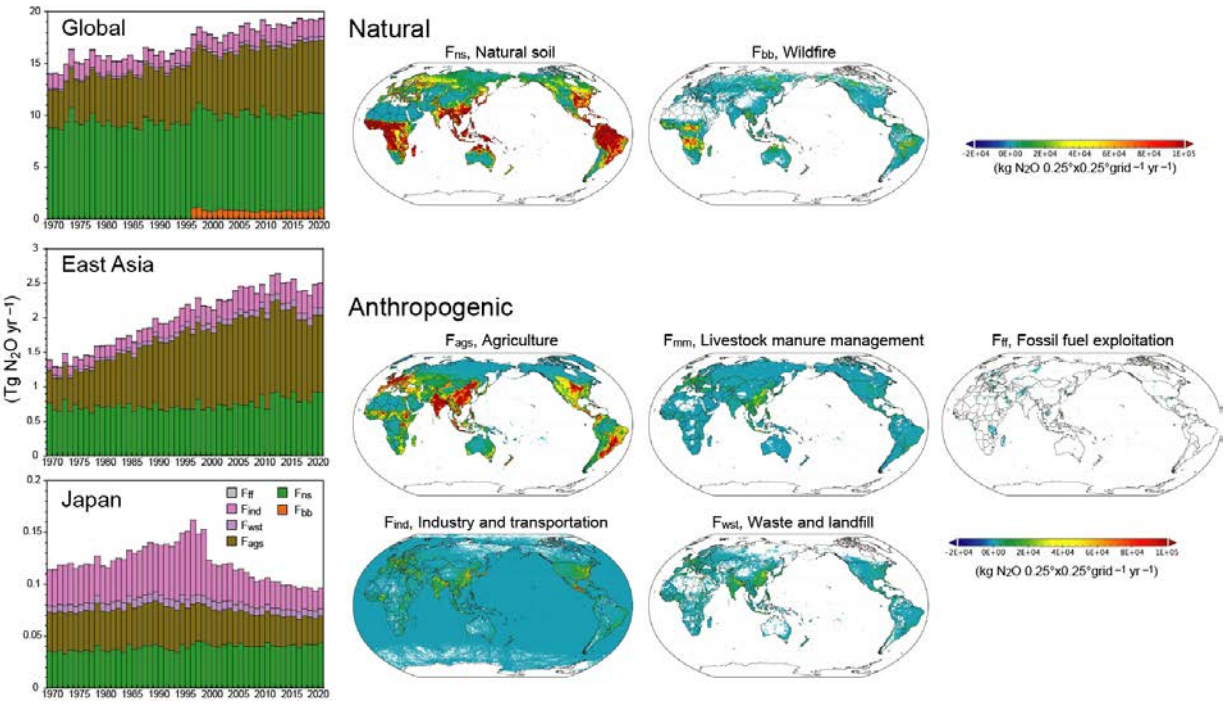

Figure 14. N_2O budgets estimated by the bottom-up approach.

3.3. Comparison between top-down and bottom-up estimates

The differences in the GHG budgets between the top-down and bottom-up approaches indicate the range of uncertainties associated with the assumptions and methods. Tables 1 and 2 compare the global and regional (East Asia) GHG budgets estimated by the top-down and bottom-up approaches for 5-year periods from 1996 to 2020. Because the two approaches used different data and models, the directions and magnitudes of biases and errors differed between them. Previous studies comparing top-down and bottom-up results have suggested that fundamental, conceptual (or terminological) differences between

the two approaches may exert substantial influences. For example, ambiguity remains in the definitions of "natural" and "anthropogenic" emissions in that land-use and biomass-burning emissions can occur heterogeneously in space and time and for various reasons. Also, in both top-down and bottom-up approaches, it is still difficult to include lateral flows such as riverine export and the transport of agricultural products and harvested wood. These issues are topics to be considered by the carbon cycle and greenhouse gas research communities.

In this report, to avoid conceptual ambiguity and to ensure accuracy in the comparison between the results obtained by the two approaches, we adopted the following definitions: For CO_2, fossil fuel combustion emissions are considered anthropogenic emissions, and net ecosystem production and land-use emissions are net natural emissions (including sinks). These definitions avoid the difficulty and uncertainty associated with the specification of land-use emissions from forest and grassland areas. For CH_4 and N_2O, total global and regional budgets, including both natural and anthropogenic emissions, are compared, because these gases have a wide variety of emission sources that are difficult to distinguish on the basis of atmospheric information. Despite these simplifications, the comparisons presented here are still useful for evaluating the consistency of our GHG budgets, especially in terms of their applicability to the GST.

Table 1. Comparison of global land total GHG budgets between top-down and bottom-up approaches (mean ± SD of interannual variability).

			1996–2000	2001–2005	2006–2010	2011–2015	2016–2020
CO_2	Nat. + LUC	top-down (NISMON)	−1.29 ± 1.25	−1.13 ± 1.06	−2.53 ± 0.73	−2.15 ± 1.14	−1.58 ± 0.78
		(MIROC4-ACTM)	−1.17 ± 1.02	−1.55 ± 0.64	−2.79 ± 0.49	−2.82 ± 0.83	−2.57 ± 0.68
		bottom-up	−3.01 ± 1.72	−2.48 ± 0.68	−3.45 ± 0.52	−3.95 ± 0.52	−3.84 ± 0.74
	Anthr. (FF)	bottom-up (GridFED)	6.60 ± 0.12	7.38 ± 0.46	8.55± 0.26	9.41 ± 0.11	9.59 ± 0.21
CH_4	Total Emis.	top-down (MIROC4-ACTM)	--	541.8 ± 6.2	555.7 ± 11.2	571.4 ± 9.4	595.9 ± 16.2
		bottom-up	443.4 ± 11.2	458.5 ± 7.6	486.2 ± 3.1	501.3 ± 6.1	516.0 ± 10.8
N_2O	Total	top-down (MIROC4-ACTM)	15.6 ± 0.7	15.6 ± 0.3	16.4 ± 1.0	17.0 ± 0.7	17.5 ± 0.7
		bottom-up	11.3 ± 0.5	11.2 ± 0.2	11.8 ± 0.3	11.8 ± 0.1	12.2 ± 0.1

CO_2 in Pg C yr^{-1}, CH_4 in Tg CH_4 yr^{-1}, N_2O in Tg N yr^{-1}

Table 2. Comparison of East Asia land total GHG budgets between top-down and bottom-up approaches (mean ± SD of interannual variability).

			1996–2000	2001–2005	2006–2010	2011–2015	2016–2020
CO_2	Nat. + LUC	top-down (NISMON)	−0.23 ± 0.20	−0.07 ± 0.24	−0.13 ± 0.38	−0.02 ± 0.22	0.25 ± 0.14
		top-down (MIROC4-ACTM)	--	−0.24 ± 0.17	−0.45 ± 0.14	−0.44 ± 0.07	-0.49 ± 0.10
		bottom-up	−0.32 ± 0.09	−0.31 ± 0.11	−0.31 ± 0.06	−0.43 ± 0.10	−0.53 ± 0.08
	Anthr. (FF)	bottom-up (GridFED)	1.44 ± 0.03	1.79 ± 0.27	2.56 ± 0.21	3.20 ± 0.05	3.27 ± 0.09
CH_4	Total Emis.	top-down (MIROC4-ACTM)	--	40.0 ± 2.5	46.1 ± 2.1	48.7 ± 3.3	49.5 ± 3.2
		bottom-up	56.0 ± 0.6	59.1 ± 3.3	68.1 ± 1.8	73.8 ± 0.9	75.4 ± 1.9
N_2O	Total	top-down (MIROC4-ACTM)	1.48 ± 0.13	1.57 ± 0.10	1.76 ± 0.13	1.71 ± 0.12	1.75 ± 0.16
		bottom-up	1.37 ± 0.05	1.41 ± 0.06	1.51 ± 0.03	1.56 ± 0.07	1.49 ± 0.05

CO_2 in Pg C yr^{-1}, CH_4 in Tg CH_4 yr^{-1}, N_2O in Tg N yr^{-1}

3.4. Evaluation of the CO_2 emission reduction effort

Figure 15 presents the global mean surface air temperature changes simulated by MIROC-ES2L (thin lines) and FaIR-1.6.4 (bold lines). From 1850 through 2014, the models were driven by the input data that was used for CMIP6, and fossil fuel CO_2 emissions during 2015–2020 were obtained from the gridded emission data of GCP-GridFED (Jones *et al*., 2021). To assess the temperature change induced by emission reduction efforts, in the baseline scenario (pink line), it was assumed that CO_2 emissions had the same annual growth rate after 2021 as the average rate during the 2010s (1.52 Pg C yr^{-1}). Otherwise, the future scenario was the same as shared socio-economic pathway (SSP) 3-7.0. The 2010s correspond to the period before the implementation of Intended Nationally Determined Contributions and before the

significant temporal reduction of emissions caused by the COVID-19 lockdown. The SSP1-1.9 and SSP1-2.6 scenarios, which correspond to targets of +1.5 and +2.0 degrees Celsius, respectively, were used for the climate projections of the emission reduction cases. The simulations demonstrated that in SSP1-1.9 and SSP1-2.6 the global surface air temperature begin to deviate from that of the baseline scenario in the late 2030s. Considering the interannual variability of global temperature, which can be captured by the full ESM, but not by the emulator, the timing at which the emission reduction effort will be clearly detected in the observed temperature is likely to be delayed.

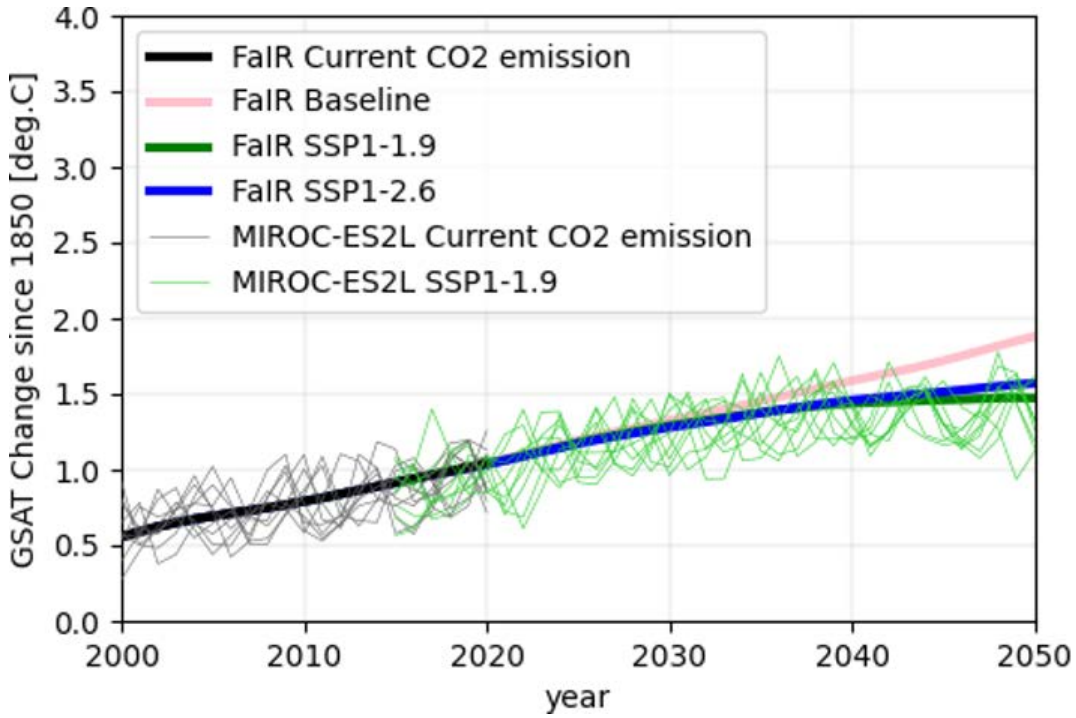

Figure 15. Global surface air temperature changes simulated by MIROC-ES2L (thin lines, 10-member results) and FaIR-1.6.4 (thick lines). The period 1850–2020 corresponds to the "historical" experiment (black line); all forcing datasets during 1850–2014 were the same as those used for CMIP6. The end of the historical experiment was extended based on the fossil fuel CO_2 emissions of 2014–2020 (GCP) and applying SSP3-7.0-prescribed emissions and/or concentrations for other species. In the historical experiment, the CO_2 concentration is nudged to the observation-based concentration. The period 2021–2050 corresponds to the three, scenario-based simulations: (1) baseline scenario (pink line), (2) SSP1-1.9 (green line), and (3) SSP1-2.6 (blue line). Anthropogenic CO_2 emissions in the baseline scenario were developed by assuming that the rate of emission growth in the 2010–2019s was maintained subsequently.

4. Concluding remarks

This report presents the global, regional, and national GHG budgets created using observational data and models for the purpose of providing evidence to the GST of the Paris Agreement based on the best available science. The GHG monitoring system proposed by the SII-8 project adequately captured spatial and temporal properties of the GHG budgets, allowing us to detect mitigation efforts and leakages in an objective and transparent manner. The system covers well the Asia-Pacific region, complementing activities in other regions such as the Copernicus and Integrated Carbon Observation System in Europe and the North American Carbon Program. Note that the present GHG budget estimates were obtained by using our own observational and model simulation data in conjunction with open datasets (e.g., emission inventories and satellite products). Through collaborative work from monitoring to modeling, the project enables us to quickly report to stakeholders (Fig. 16). There remain, nevertheless, substantial uncertainties due to sparse observational coverage, errors in immature models, and biased emission inventories. Fortunately, through ongoing efforts, the project is expected to overcome these limitations and provide more reliable GHG budgets in support of the transparent accomplishment of the GST.

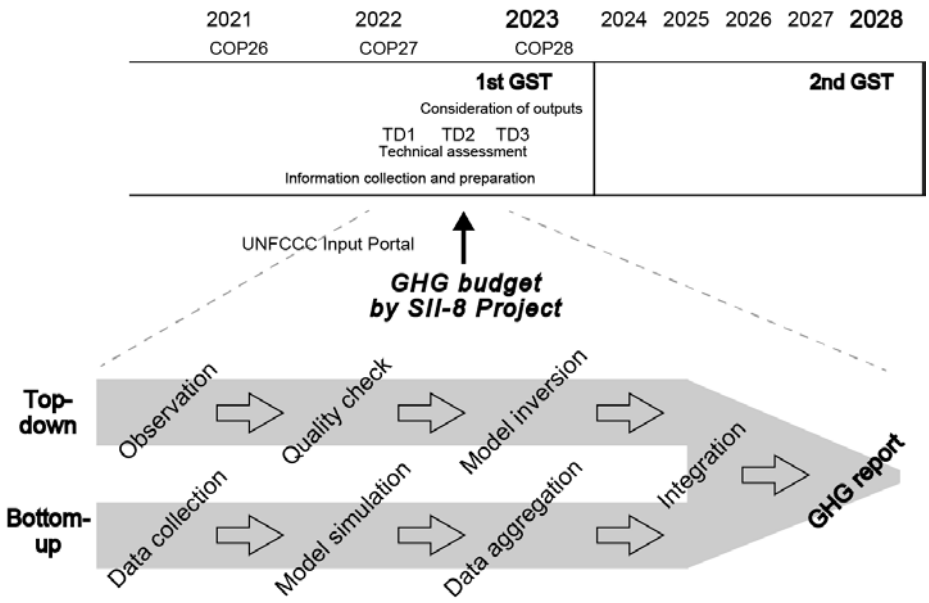

Figure 16. Expected timeline of GHG budget contributions to the Global Stocktake (GST).

Corresponding GST1 Guiding Questions (by SB chairs, ver. 18 Feb. 2022) and our answers

<Mitigation>

Q1. *What is the collective progress in terms of the current implementation of, and ambition in, mitigation actions towards achieving the goals defined in Articles 2.1(a)1 and 4.12 of the Paris Agreement?*

A1. We have achieved progress in GHG monitoring with regard to comprehensive and rapid evaluation and reporting, as demonstrated in this report, to support the accomplishment of the mitigation goals.

Q2. *Taking into account nationally determined contributions, long-term low GHG emission development strategies and relevant commitments and initiatives, what are the projected global GHG emissions, and the emission reductions still needed, in 2030 and 2050 in order to achieve the goals defined in Articles 2.1(a) and 4.1 of the Paris Agreement?*

A2. To prevent global warming well below 1.5°C above pre-industrial levels, net zero emission should be achieved by 2050 or earlier. The GHG monitoring system demonstrated in this report is expected to support the accomplishment of this goal by providing scientific evidence for projected emissions and emission reductions.

Q3. *What efforts are being undertaken to plan, implement and accelerate mitigation action towards achieving the goals defined in Articles 2.1(a) and 4.1 of the Paris Agreement?*

A3. More efforts are needed to evaluate country-level GHG budgets with adequate transparency, which can be accomplished through internationally coordinated observations and analyses.

Q4. *How adequate and effective are the current mitigation efforts and support provided for mitigation action towards achieving Articles 2.1(a) and 4.1 of the Paris Agreement?*

A4. Current mitigation efforts are insufficient to achieve the net zero emission and 1.5°C global warming goals, and the scientific community is required to establish and maintain GHG monitoring systems to verify the mitigation efforts.

Q5. *In order achieve the goals defined in Articles 2.1(a) and 4.1 of the Paris Agreement:*

a) What further action is required?

A5-a. In addition to mitigation efforts, the establishment of an internationally coordinated GHG monitoring system is required for transparency.

b) What are the barriers and challenges, and how can they be addressed at national, regional and

international levels?

A5-b. In GHG monitoring, there remain observational gaps (e.g., tropical forests and the Southern Ocean) and model biases that threaten the reliability of the estimation. Decreasing the magnitudes of these gaps and biases is a challenge for the scientific community.

c) What are the opportunities, good practices, lessons learned and success stories?

A5-c. Establishing a comprehensive, internationally coordinated GHG monitoring system is beneficial for both the scientific community and climate policies.

<Cross-cutting>

Q20. *How are Parties recognizing the importance of ensuring the integrity of all ecosystems, including oceans, and the protection of biodiversity, in order to achieve the purpose and long-term goals of the Paris Agreement?*

A20. The GHG monitoring system proposed here includes ecosystem GHG exchanges such as photosynthetic CO_2 uptake and biomass burning emissions. These observational data can be useful for evaluating ecosystem integrity at local to global scales through time.

Acknowledgments

The project SII-8 "Comprehensive Study on Multi-scale Monitoring and Modeling of Greenhouse Gas Budgets" is funded by the Ministry of the Environment of Japan (JPMEERF21S20800). MIROC-ES2L development and simulations for CMIP6 are supported by the TOUGOU Project, Ministry of Education, Culture, Sports, Science, and Technology. MIROC4-ACTM inversion activity is partly supported by the Arctic Challenge for Sustainability II project (ArCS-II; JPMXD1420318865).

Data availability

- CONTRAIL-CME
  - CO_2: https://www.nies.go.jp/doi/10.17595/20210827.001-e.html
- Hateruma Station observation data
  - CO_2: http://www.nies.go.jp/doi/10.17595/20160901.001-e.html
  - CH_4: http://www.nies.go.jp/doi/10.17595/20160901.003-e.html
- MIROC4-ACTM data
  - CO_2: https://doi.org/10.5281/zenodo.5776197, https://doi.org/10.5281/zenodo.5776212
  - CH_4: https://doi.org/10.5281/zenodo.5920070
  - N_2O: https://doi.org/10.5281/zenodo.5889524
- NISMON-CO_2
  - CO_2: https://www.nies.go.jp/doi/10.17595/20201127.001-e.html
- VISIT output
  - CO_2, CH_4, N_2O: https://www.nies.go.jp/doi/10.17595/20210521.001-e.html

References

Akagi SK, et al. (2011) Emission factors for open and domestic biomass burning for use in atmospheric models. Atm Chem Phys 11, 4039–4072. DOI: 10.5194/acp-22-9215-2022

Bisht JSH, et al. (2021) Seasonal variations of SF_6, CO_2, CH_4, and N_2O in the UT/LS region due to emissions, transport, and chemistry. J Geophys Res Atm, 126, e2020JD033541. DOI: 10.1029/2020JD033541

Chandra N, et al. (2021) Emissions from the oil and gas sectors, coal mining and ruminant farming drive methane growth over the past three decades. J Meteor Soc Jpn, 99, 309–337. DOI: 10.2151/jmsj.2021-015

Chandra N et al. (2022) Estimated regional CO_2 flux and uncertainty based on an ensemble of atmospheric CO_2 inversions. Atmos Chem Phys, 22, 9215–9243, DOI: 10.5194/acp-22-9215-2022

Crippa M, et al. (2020) High resolution temporal profiles in the emissions database for global atmospheric research. Scientific Data 7, 121. DOI: 10.1038/s41597-020-0462-2

Friedlingstein P, et al. (2022) Global carbon budget 2022. Earth System Sci Data, 14, 4811–4900. DOI: 10.5194/essd-14-4811-2022

Hajima T, et al. (2020) Development of the MIROC-ES2L Earth system model and the evaluation of biogeochemical

processes and feedbacks. Geosci Model Dev 13, 2197–2244. DOI: 10.5194/gmd-13-2197-2020
Iida Y, et al. (2021), Global trends of ocean CO_2 sink and ocean acidification: an observation-based reconstruction of surface ocean inorganic carbon variables. J Oceanogr, 77, 323–358. DOI:10.1007/s10872-020-00571-5
Inatomi, M., A. Ito, K. Ishijima, S. Murayama (2010) Greenhouse gas budget of a cool temperate deciduous broadleaved forest in Japan estimated using a process-based model. Ecosystems, 13, 472–483, DOI: 10.1007/s10021-010-9332-7
Ishii M, et al. (2011), Ocean acidification off the south coast of Japan: A result from time series observations of CO_2 parameters from 1994 to 2008, J Geophys Res, 116, C06022. DOI: 10.1029/2010JC006831
Ito A (2019) Disequilibrium of terrestrial ecosystem CO_2 budget caused by disturbance-induced emissions and non-CO_2 carbon export flows: a global model assessment. Earth System Dyn, 10, 685–709. DOI: 10.5194/esd-10-685-2019
Ito A, Inatomi M (2012) Use of a process-based model for assessing the methane budgets of global terrestrial ecosystems and evaluation of uncertainty. Biogeosci, 9, 759–773. DOI: 10.5194/bg-9-759-2012
Ito A, et al. (2018) Emissions of nitrous oxide (N_2O) from soil surfaces and their historical changes in East Asia: a model-based assessment. Progr Earth Planet Sci, 5. DOI: 10.1186/s40645-018-0215-4
Jones MW, et al. (2021) Gridded fossil CO_2 emissions and related CO_2 combustion consistent with national inventories 1959–2018. Sci Data, 8, 2. DOI: 10.1038/s41597-020-00779-6
Kobayashi S, et al. (2015) The JRA-55 reanalysis: General specification and basic characteristics. J Meteor Soc Jpn, 93, 5–48. DOI: 10.2151/jmsj.2015-001
Machida T, et al. (2008) Worldwide measurements of atmospheric CO_2 and other trace gas species using commercial airlines. J Atm Ocean Technol, 25, 1744–1754. DOI: 10.1175/2008JTECHA1082.1
Matsueda H, et al. (2008) Evaluation of atmospheric CO_2 measurements from new flask air sampling of JAL airliner observations. Papers Meteorol Geophys, 59, 1–17. DOI:10.2467/mripapers.59.1
Millar RJ, Nicholls ZR, Friedlingstein P, Allen MR (2017) A modified impulse-response representation of the global near-surface air temperature and atmospheric concentration response to carbon dioxide emissions. Atm Chem Phys, 17, 7213–7228.
Mukai Y, et al. (2001) Characterization of atmospheric CO_2 observed at two-background air monitoring stations (Hateruma and Ochiishi) in Japan. In Sixth International Carbon Dioxide Conference (ed. Nakazawa, T.)
Nicholls ZRJ, et al. (2020). Reduced Complexity Model Intercomparison Project Phase 1: introduction and evaluation of global-mean temperature response. Geosci Model Dev, 13, 5175–5190. DOI: 10.5194/gmd-13-5175-2020.
Niwa Y (2020) Long-term global CO_2 fluxes estimated by NICAM-based Inverse Simulation for Monitoring CO_2 (NISMON-CO_2), ver.2022.1, Center for Global Environmental Research, NIES. DOI:10.17595/20201127.001, (Reference date: 2022/12/27)
Niwa Y, et al. (2011) Three-dimensional variations of atmospheric CO_2: aircraft measurements and multi-transport model simulations. Atm Chem Phys, 11, 13359–13375. DOI: 10.5194/acp-11-13359-2011
Niwa Y, et al. (2017a) A 4D-Var inversion system based on the icosahedral grid model (NICAM-TM 4D-Var v1.0) – Part 1: Offline forward and adjoint transport models. Geosci Model Dev, 10, 1157–1174. DOI: 10.5194/gmd-10-1157-2017
Niwa Y, et al. (2017b), A 4D-Var inversion system based on the icosahedral grid model (NICAM-TM 4D-Var v1.0) – Part 2: Optimalization scheme and identical twin experiment of atmospheric CO_2 inversion, Geosci Model Dev, 10, 2201–2219. https:/doi.org/10.5194/gmd-10-2201-2017
Niwa Y, et al. (2021) Estimation of fire-induced carbon emissions from Equatorial Asia in 2015 using in situ aircraft and ship observations. Atm Chem Phys, 21, 9455–9473. DOI: 10.5194/acp-21-9455-2021
Niwa Y, Ishijima K, Ito A, Iida Y (2022) Toward a long-term atmospheric CO_2 inversion for elucidating natural carbon fluxes: technical notes of NISMON-CO_2 v2021.1, Prog. Earth Planet Sci., 9, 42. DOI: 10.1186/s40645-022-00502-6
Ono H, et al. (2019) Acceleration of ocean acidification in the Western North Pacific. Geophys Res Lett, 46, 13161–13169. DOI: 10.1029/2019GL085121
Patra PK, et al. (2011) TransCom model simulations of CH_4 and related species: linking transport, surface flux and chemical loss with CH_4 variability in the troposphere and lower stratosphere. Atm Chem Phys, 11, 12813–12837. DOI: doi:10.5194/acp-11-12813-2011
Patra PK, et al. (2016) Regional methane emission estimation based on observed atmospheric concentrations (2002–2012). J Meteor Soc Jpn, 94, 91–113. DOI: 10.2151/jmsj.2016-006
Patra PK, et al. (2018) Improved chemical tracer simulation by MIROC4.0-based Atmospheric Chemistry-Transport Model (MIROC4-ACTM). SOLA, 14, 91–96. DOI: 10.2151/sola.2018-016
Patra PK, et al. (2022) Forward and inverse modelling of atmospheric nitrous oxide using MIROC4-atmospheric chemistry-transport model. J Meteorol Soc Jpn, 100. DOI:10.2151/jmsj.2022-018

Saeki T, Patra PK (2017) Implications of overestimated anthropogenic CO_2 emissions on East Asian and global land CO_2 flux inversion. Geosci Lett, 4, DOI: 10.1186/s40562-017-0074-7
Satoh M, et al. (2014) The Non-hydrostatic Icosahedral Atmospheric Model: description and development. Progr Earth Planet Sci, 1, 18. DOI: 10.1186/s40645-014-0018-1
Smith C, et al. (2018) FAIR v1.3: a simple emission-based impulse response and carbon cycle model. Geosci Model Dev, 11, 2273-2297. DOI: 10.5194/gmd-11-2273-2018
Terao Y, et al. (2011) Interannual variability and trends in atmospheric methane over the western Pacific from 1994 to 2010. J Geophys Res 116: DOI:10.1029/2010JD15467
Tohjima Y, et al. (2002) Analysis and presentation of in situ atmospheric methane measurements from Cape Ochi-ishi and Hateruma Island. J Geophys Res, 107, 4148. DOI: 10.1029/2001JD001003
Tohjima Y, et al. (2012) Analysis of seasonality and annual mean distribution of atmospheric potential oxygen (APO) in the pacific region. Global Biogeochem Cycles, 26. DOI: 10.1029/2011GB004110
Tohjima Y, et al. (2014) Temporal changes in the emissions of CH_4 and CO from China estimated from CH_4 / CO_2 and CO / CO_2 correlations observed at Hateruma Island. Atm Chem Phys, 14, 1663–1677. DOI: 10.5194/acp-14-1663-2014
Tohjima Y, et al. (2020) Detection of fossil-fuel CO_2 plummet in China due to COVID-19 by observation at Hateruma. Sci Rep, 10, 18688. DOI: 10.1038/s41598-020-75763-6
Tohjima Y, et al. (2022) Did atmospheric CO_2 and CH_4 observation at Yonagunijima detect fossil-fuel CO_2 reduction due to COVID-19 lockdown? J Meteor Soc Japan, 100, 437–444. DOI: 10.2151/jmsj.2022-021
Tohjima Y, et al. (2023) Near-real-time estimation of fossil fuel CO_2 emissions from China based on atmospheric observations on Hateruma and Yonaguni Islands, Japan. Prog Earth Planet Sci (accepted on Feb. 17, 2023). DOI: 10.1186/s40645-023-00542-6
Tsuboi K, et al. (2013), Evaluation of a new JMA aircraft flask sampling system and laboratory trace gas analysis system. Atm Measur Tech, 6, 1257–1270, DOI: 10.5194/amt-6-1257-2013
Tsuboi K, et al. (2017), Inter Comparison Experiments for Greenhouse Gases Observation (iceGGO) in 2012–2016, Tech Rep Meteorol Res Inst. No.79. DOI: 10.11483/mritechrepo.79
Tsutsumi Y, et al. (2006) Long-term trends of greenhouse gases in regional and background events observed during 1998–2004 at Yonagunijima located to the east of the Asian continent. Atm Env, 40, 5868–5879. DOI: 10.1016/j.atmosenv.2006.04.036
Umezawa T, et al. (2020) Statistical characterization of urban CO_2 emission signals observed by commercial airline measurements. Sci Rep, 10, 7963. DOI: 10.1038/s41598-020-64769-9
van der Werf GR, et al. (2017) Global fire emissions estimates during 1997–2016. Earth Sys Sci Data, 9, 697–720. DOI: 10.5194/essd-9-697-2017
Watanabe F, et al. (2000) Interannual variation of growth rate of atmospheric carbon dioxide concentration observed at the JMA's three monitoring stations: Large increase in concentration of atmospheric carbon dioxide in 1998. J Meteorol Soc Jpn, 78, 673–682. DOI: 10.2151/jmsj1965.78.5_673
Wolter K, Timlin MS (2011), El Niño / Southern Oscillation behaviour since 1871 as diagnosed in an extended multivariate ENSO index (MEI.ext). Int J Climatol, 31, 1074–1087. DOI: 10.1002/joc.2336
Yokota T, et al. (2009) Global Concentrations of CO_2 and CH_4 retrieved from GOSAT: First Preliminary Results. SOLA, 5, 160–163. DOI: 10.2151/sola.2009-041
Yoshida Y, et al. (2013) Improvement of the retrieval algorithm for GOSAT SWIR XCO_2 and XCH_4 and their validation using TCCON data. Atm Measur Tech, 6, 1533–1547. DOI: 10.5194/amt-6-1533-2013

Contacts

International Coordination Office, National Institute for Environmental Studies, Japan

Notes:

ppm: parts per million, abbreviating a dry air mole fraction of 10^{-6} mol mol^{-1}
Pg: petagram (10^{15} g)
Tg: teragram (10^{12} g)
EDGAR: Emission Data for Global Atmospheric Research
GFED: Global Fire Emission Database
MIROC: Model for Interdisciplinary Research on Climate
NICAM: Nonhydrostatic Icosahedral Atmospheric Model
VISIT: Vegetation Integrative SImulator for Trace gases